Bull. Mater. Sci., Vol. 32, No. 1, February 2009, pp. 23–30. © Indian Academy of Sciences.

Preparation and characterization of nanostructured ZnO thin films for photoelectrochemical splitting of water

MONIKA GUPTA, VIDHIKA SHARMA, JAYA SHRIVASTAVA, ANJANA SOLANKI, A P SINGH†, V R SATSANGI†, S DASS and ROHIT SHRIVASTAV*

Department of Chemistry, †Department of Physics and Computer Science, Dayalbagh Educational Institute, Dayalbagh, Agra 282 005, India

MS received 21 June 2006; revised 27 November 2008

Abstract. Nanostructured zinc oxide thin films (ZnO) were prepared on conducting glass support (SnO_2: F overlayer) via sol–gel starting from colloidal solution of zinc acetate 2-hydrate in ethanol and 2-methoxy ethanol. Films were obtained by spin coating at 1500 rpm under room conditions (temperature, 28–35°C) and were subsequently sintered in air at three different temperatures (400, 500 and 600°C). The evolution of oxide coatings under thermal treatment was studied by glancing incidence X-ray diffraction and scanning electron microscopy. Average particle size, resistivity and bandgap energy were also determined. Photoelectrochemical properties of thin films and their suitability for splitting of water were investigated. Study suggests that thin films of ZnO, sintered at 600°C are better for photoconversion than the films sintered at 400 or 500°C. Plausible explanations have been provided.

Keywords. Nanostructured thin film; zinc oxide; sol–gel; photoelectrochemical cell; water splitting.

1. Introduction

Low dimensional nanostructured materials are of great interest due to their unique physical and chemical properties. Among these, zinc oxide (ZnO) is a wide bandgap semiconductor with a direct bandgap of 3·2–3·36 eV at room temperature and exciton binding energy of 60 meV (Wang *et al* 2007). Most prominent crystalline structure of ZnO is wurtzite type, although, it also exists in the cubic zincblende and rocksalt structures. In wurtzite type, a hexagonal lattice (lattice parameters, $a = 3{\cdot}24$ Å and $c = 5{\cdot}16$ Å) with space group $P6_3mc$ is characterized by two interconnecting sublattices of Zn^{2+} and O^{2-}, such that each Zn ion is surrounded by a tetragonal coordination. This gives rise to polar symmetry along the hexagonal axis, which is responsible for a number of properties of ZnO, viz. piezoelectricity and spontaneous polarization, and is a key factor in crystal growth and defect generation. ZnO has a very rich defect chemistry also with prominent point or one-dimensional defects, which include mostly oxygen vacancies and zinc interstitials. Owing to such defects ZnO shows a broad low intensity spectrum centred at green colour wavelength from 400–700 nm approximately, besides the high intensity peak at the UV wavelength (> 400 nm) (Ashrafi and Jagdish 2007).

Thin films of ZnO have been widely used in transparent electrodes, surface acoustic wave devices, field effect transistors and display devices (Sagar *et al* 2005). It can be a cheaper substitute to GaN for optoelectronic applications in the blue and UV regions (Lu *et al* 2007). Nanoscale porous structures of ZnO with a high surface area find applications in chemical sensors and solar cells (Musat *et al* 2008). Thin films of doped/undoped ZnO can be obtained by various techniques such as spray pyrolysis, organometallic chemical vapour deposition, pulsed laser deposition, sputtering, and sol–gel process. However, obtaining ZnO films with superior optical and electrical properties suitable for device applications is still a technological challenge. Several new approaches, use of variety of substrates and experimental conditions are enabling a wide range of optical and electrical properties in ZnO thin films.

Research on photoelectrochemical (PEC) cells, particularly their use in solar energy conversion, has gained importance in the last few decades (Chandra Babu *et al* 1994). PEC cells convert solar energy into storable chemical energy as hydrogen through the photoelectrolysis of water. A semiconductor, used as photoelectrode in PEC cell, must be chemically stable with an optimum bandgap (≈ 1·8 eV) enabling it to absorb visible part of solar radiations (Agrawal *et al* 2003; Chauhan *et al* 2006). Semiconductors viz. TiO_2 (Yoko *et al* 1991), $SrTiO_3$ (Salvador *et al* 1984), SnO_2 (Yoon and Chung 1992) and $BaTiO_3$ (Stilwell and Park 1982), investigated

*Author for correspondence (rohitshrivastav_dei@yahoo.co.in)

as alternative photoelectrodes, are of relatively high bandgap and cannot absorb large portion of visible light. On the other hand, low bandgap materials viz. Si (Levy-Clement *et al* 1991), GaAs (Fu-Ren Fan and Bard 1980) and InP (Chandra *et al* 1985) get easily corroded in contact with the electrolyte. Despite its high bandgap (figure 1), ZnO is an attractive material for PEC splitting of water mainly due to its high electrochemical stability. The energy levels and bandgap energy of ZnO are quite similar to TiO_2, which is the first material reported for PEC splitting of water. The conduction and valence band edges of ZnO straddle H_2O/H_2 and OH^-/O_2 redox levels and, thus, satisfy a mandatory requirement for spontaneous photosplitting of water. Further, electron mobility in ZnO is much higher than that of TiO_2 and it can be an advantage for fabricating PEC/solar cells. Moreover, defects induced low intensity absorption in visible region can be exploited to convert ZnO into a good solar light absorber.

Nanostructured materials, in contrast to their bulk counterparts, exhibit significant alteration in their properties viz. bandgap, porosity and surface area, which are crucial for PEC applications (Armelao *et al* 2003; Chaudhary *et al* 2004; Morales *et al* 2005). The idea of exploiting nanomaterials to achieve efficient PEC splitting of water has been coined recently (Chauhan *et al* 2006). Nanostructured ZnO is one of the materials for this purpose but not many reports exist, so far, exploring this aspect. This report deals with the preparation of thin films of nanostructured ZnO by sol–gel spin coating, their structural and optical characterization and study on their possible application in PEC splitting of water.

2. Experimental

2.1 *Preparation of thin films of zinc oxide*

The starting compound in this study was zinc acetate 2-hydrate. The choice was made taking into account the fact that hydrolysis of acetate group gives products which are soluble in the solvent medium and get easily decomposed into volatile compounds under heat treatment (Armelao *et al* 2003). A colloidal solution of zinc acetate 2-hydrate (0·2 M) was prepared by refluxing it for 3 h at 80°C in dry ethanol. Subsequently 2-methoxy ethanol and ethanol were added to adjust the final concentration in the range 0·05–0·2 M. The resulting precursor solution was kept overnight for stabilization and used to deposit film. Films were obtained by spin-coating at 1500 rpm. The solvent evaporation, accompanied by further condensation reactions, resulted in deposition of a solid film onto the substrate. Film samples were sintered at 400, 500 and 600°C for 1 h in muffle furnace, in air. The sintered films were homogeneous, well adherent to the substrate and were free from cracks and pinholes. When compared to conventional thin film forming processes, such as, chemical vapour deposition, evaporation, or sputtering, the sol–gel spin-coating requires considerably less equipment and is potentially less expensive. Besides, in this method the microstructure of the deposited film can be easily tailored by regulating the preparation conditions viz. solution concentration, annealing temperature, and annealing environment (Oral *et al* 2004). TCO glass plates (having SnO_2: F overlayer on one side) were used as substrate, which were washed, before film deposition by soaking (for 2–5 min) in the following solvents in the same order: HCl, double distilled water, HF, double distilled water, acetone, double distilled water. Cleaned substrates (3 × 2 cm) were dried in an oven at 40°C and stored in moisture and dust-free environment by placing inside an air-tight glass container. Films were deposited, at room temperature only on nearly 3/4th length of substrate plates, while remaining portion of substrate was reserved for establishing electrical contact, when such films were converted into electrodes.

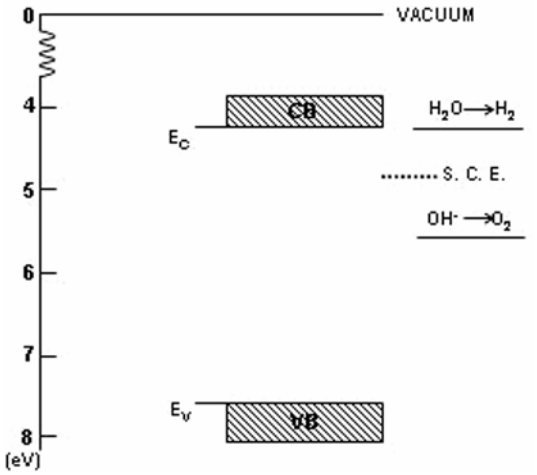

Figure 1. Energy band diagram of ZnO.

2.2 *PEC study*

Films were used as working electrodes (WE) in PEC cells. To develop WE an ohmic electrical contact was created from one edge of the substrate (where film was not deposited) with silver paint and a copper wire. Excluding an area of 2·25 cm^2 (1·5 × 1·5 cm) at the centre of the film, all edges and electrical contact were sealed by a non-transparent, non-conducting epoxy resin, hysol (Dexter, Singapore). PEC studies were conducted using three-electrode configuration electrochemical cell, which had a pyrex window for incoming radiations, and a water jacket, around it, to prevent heating effects. The semiconductor, WE, was used in association with a platinum foil counter electrode (CE) and saturated calomel reference electrode (SCE). Aqueous solution of NaOH (pH = 13), was used as electrolyte and this solution was purged with N_2 for 15–20 min just before PEC study. A Potentiostat (Model

ECDA-001, Conserv Enterprises) and a 150 W Xenon Arc lamp (Oriel, USA, used as light source) were employed to record current–voltage (I–V) characteristics of the cell, both under darkness and illumination. The variation in capacitance with applied bias voltage, under darkness, was also recorded by employing LCR meter (Model 4263 B, Agilent Technologies), and the data was utilized to evaluate the values of flat band potential and charge carrier density.

Reagents with purity > 99·9% and double distilled deionized water (specific conductance < 10^{-6} mho cm^{-1}) were used throughout the study. Film samples were prepared in triplicate and with each sample 3–5 repetitive measurements were recorded.

3. Results and discussion

In this study zinc acetate (Ac) 2-hydrate, [$Zn(CH_3COO)_2{\cdot}2H_2O$], was the starting material for the growth of ZnO thin films by the sol-gel process (Kim *et al* 2003). The chemical reactions for Zn in this process were as follows:

$$Zn(Ac)_2{\cdot}2H_2O \quad Zn(Ac)_2 + 2H_2O, \qquad (I)$$

$$Zn(Ac)_2 + 2OR\text{-}OH \quad Zn(OR)_2 + 2Ac\text{-}OH, \qquad (II)$$

$$Zn(OR)_2 + 2H_2O \quad Zn(OH)_2 + 2R\text{-}OH, \qquad (III)$$

$$Zn(OH)_2 \quad ZnO + H_2O. \qquad (IV)$$

All film samples were found to be of n-type which might be related to O vacancy and/or Zn interstitials probably due to nonstoichiometric growth (Ashrafi and Jagdish 2007). Data presented in table 1 indicate that resistivity of ZnO films decreased on increasing the sintering temperature from 400–600°C. Film thickness was found to be in the range of 2·37–2·83 μm. Measured density of films ranged from 2·24–2·69 g cm^{-3}, which is ≈ 40–48% of theoretical density (5·60 g cm^{-3}) of ZnO. This suggests that the films are porous and can provide a larger contact area with electrolyte when used in PEC cell.

Table 1. Measured resistivity and thickness of zinc oxide films.

	Thickness* (μm)	Resistivity* (kΩ cm)
Sintering temperature (°C)	Mean ± SD	Mean ± SD
400	2·83 ± 0·05	15·6 ± 1·3
500	2·46 ± 0·04	12·8 ± 1·1
600	2·37 ± 0·04	9·3 ± 0·8

*Values represent a mean of 10–15 observations; SD: Standard deviation

Thin films of zinc oxide were subjected to phase analysis by employing X-ray diffractometer (Philips, Model: X'PERT PW3020), that was equipped with graphite monochromator, a mirror at a fixed incidence angle of 1·5° and CuKα-1 as radiation source (λ = 1·542 Å). The angular accuracy was 0·001° and the angular resolution was better than 0·01°. Figure 2 shows glancing angle X-ray diffraction patterns of zinc oxide films obtained at different sintering temperatures and reveal polytypism in the samples. The peaks at 2θ angle 33·7, 37·7 and 54·6° with d_{hkl} 2·66, 2·39 and 1·65 Å correspond to diffraction from planes (002), (101) and (110), respectively, of hexagonal wurtzite ZnO. Similarly, peaks at 2θ angle 52·5, 61·6 and 66·4° with d_{hkl} 1·74, 1·51 and 1·41 Å are due to diffraction from planes (200), (220) and (222), respectively, of cubic zincblende ZnO. Thermodynamically ZnO is stable with the wurtzite phase due to its ionicity that resides exactly at the borderline between the covalent and the ionic materials. However, the total energy of wurtzite ZnO is lower than that of zincblende phase only by 50 meV, which indicates that there exists the possibility of obtaining metastable zincblende ZnO also. In fact, evolution of zincblende ZnO by sol–gel process was reported even earlier (Kim *et al* 2003). Although, zincblende ZnO is a metastable phase, yet there is a strong possibility to have phase mixture or wurtzite subdomains embedded in the zincblende matrix (Ashrafi and Jagdish 2007). The present study confirms this possibility. So far, there is no report on how to reduce or control the evolution of wurtzite subdomains in the zincblende ZnO matrix. It is, thus, clear that a complex microstructural evolution occurs under annealing in zinc oxide films, which is guided by several inter-related and obscure parameters. Further, the presence of multiple peaks of the ZnO phase indicates the polycrystalline nature of films (Maruyama 1998). In earlier studies, ZnO films obtained by molecular beam RF sputtering and sol–gel were also reported to be polycrys-

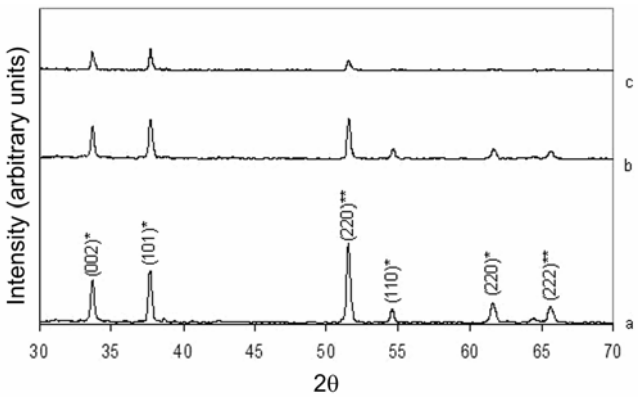

Figure 2. X-ray diffraction pattern of zinc oxide films sintered at: a. 400, b. 500 and c. 600°C (*peaks corresponding to hexagonal wurtzite ZnO; **peaks corresponding to cubic zincblende ZnO).

Table 2. Average size of particles/grains in zinc oxide film and its variation with sintering temperature.

Sintering temperature (°C)	Particle size from Scherrer's calculation* (nm) Mean ± SD	Particle size from SEM analysis (μm)
400	28 ± 6	0·35
500	30 ± 5	0·21
600	3 ± 6	0·14

* and S.D. : same as in table 1

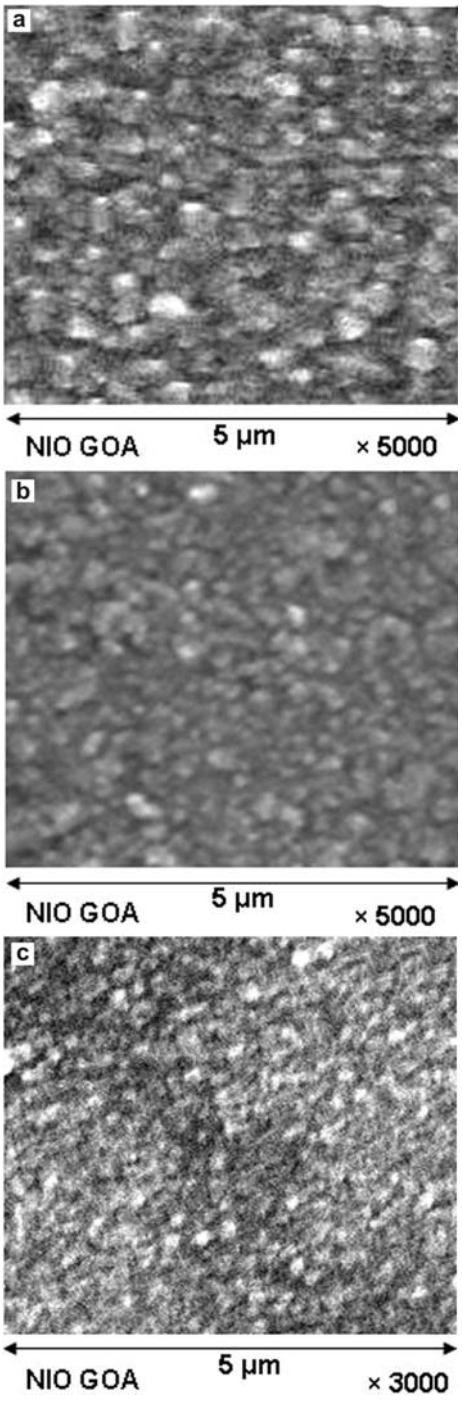

Figure 3. SEM images of zinc oxide films sintered at: **a**. 400, **b**. 500 and **c**. 600°C.

talline (Wang *et al* 2007; Musat *et al* 2008). In several studies, *c* axis oriented growth of wurtzite ZnO grains is seen (Musat *et al* 2008). But the relative intensities of the peaks in the XRD pattern, in this study, suggest that there is no grain orientation in the samples (Oral *et al* 2004). With the increase in sintering temperature of film from 400 through 600°C, the crystalline character of ZnO decreases as is indicated by smaller width of peaks (Armelao *et al* 2003).

Utilizing the X-ray diffraction data, the average particle/grain size in ZnO films was estimated (Klug and Alexander 1974) by Scherrer's equation,

$$t = k\lambda/B\cos\theta, \quad (1)$$

where t is grain size, B the full width at half maxima and λ the wavelength of X-ray used (1·542 Å). The computed values are presented in table 2.

Scanning electron microscope (SEM) (Model: JEOL JSMS 800LV) was used to examine the surface morphology of ZnO films and the results are shown in figure 3. In general, films are homogeneous and continuous. Separate coating layers are not visible in sintered films. There seems to be a mismatch in average size of grains/particles determined through Scherrer's calculation utilizing XRD data and SEM analysis. SEM images suggest size of grains to be much larger. Further, while Scherrer's calculation suggests an increase in particle size with rise in sintering temperature, SEM images indicate almost a reverse trend. Taking into account the above discrepancy and the fact that SEM analysis reveals formation of particles with different shapes and sizes, it seems appropriate to consider that the particles which appear in SEM images are, in fact, grain agglomerates, which get fragmented with rise in sintering temperature (Chauhan *et al* 2006). However, at even higher sintering temperature, the possibility of fusion of grain boundaries resulting in a marginal increase in particle size cannot be ruled out. Columnar growth along *c* axis in films of zinc oxide is generally reported (Ashrafi and Jagdish 2007). But no such grain elongation in a preferred direction is seen here. The random distribution of grains, in projection and size, only suggests a random nucleation mechanism, and random orientation of grains show that the grain growth is isotropic (Oral *et al* 2004).

The UV-Vis photospectra of ZnO thin films were recorded with respect to the bare substrate placed in the

reference beam using double beam spectrophotometer (Shimadzu, Model: UV-2450). Absorption spectra as a function of sintering temperature for ZnO films are shown in figure 4. The absoption at higher wavelengths in the visible region is low and at wavelength 392–414 nm an intense absorption threshold can be seen. Further, absorption increases as sintering temperature rises from 400 through 600°C. It is a known fact that decrease in optical absorption can be attributed to the improvement in crystallinity and/or variations in stoichiometry (Djaoued *et al* 1997). From XRD data shown in figure 2 the maximum crystallinity is apparent in films sintered at 400°C, while films sintered at 600°C have the lowest value of crystallinity. The rise in absorption, observed on increasing sintering temperature, can be, thus, largely attributed to the observed decrease in crystallinity, while stoichiometry has seemingly remained unaffected by variations in sintering temperature (Ahn *et al* 2007). The observed broadening of the absorption edge at higher sintering temperatures (600°C) may be due to the increase in disorder in semiconductor films, as is evident from SEM images also, which probably leads to the appearance of localized electron and/or hole states (Ahn *et al* 2007).

The spectra were analysed by plotting $(\alpha h\nu)^2$ vs $h\nu$, based on (2) (Ray 2001)

$$\alpha h\nu = A(h\nu - E_g)^{n/2}, \tag{2}$$

where α is absorption coefficient, A a constant (independent from frequency, ν) and n the exponent that de-

Table 3. Bandgap energy of zinc oxide films.

Sintering temperature (°C)	Bandgap energy* (eV)
	Mean ± SD
400	3·20 ± 0·06
500	3·19 ± 0·06
600	3·16 ± 0·05

* and SD: same as in table 1

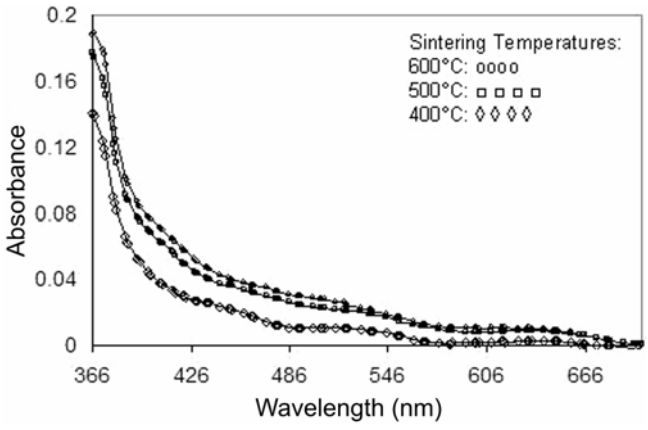

Figure 4. Plot of absorption vs wavelength for zinc oxide films sintered at different sintering temperatures.

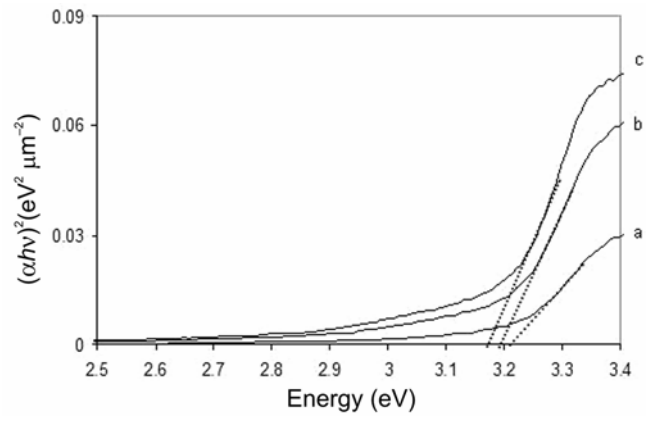

Figure 5. Plot of $(\alpha h\nu)^2$ vs $h\nu$ for zinc oxide film sintered at: a. 400, b. 500 and c. 600°C.

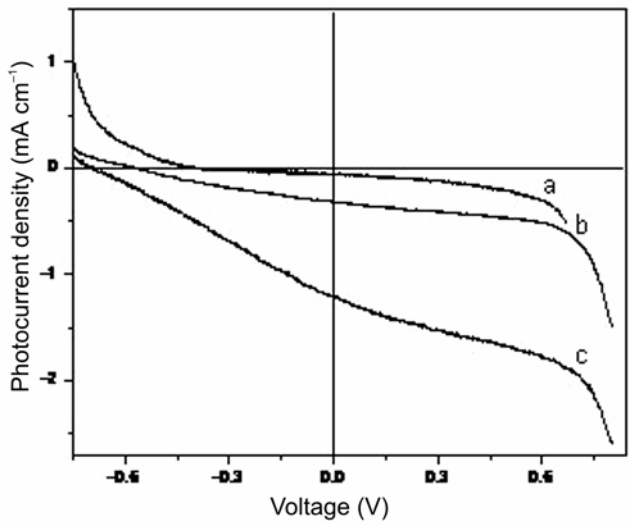

Figure 6. Variation of photocurrent density with applied voltage (vs SCE) employing films sintered at a. 400, b. 500 and c. 600°C.

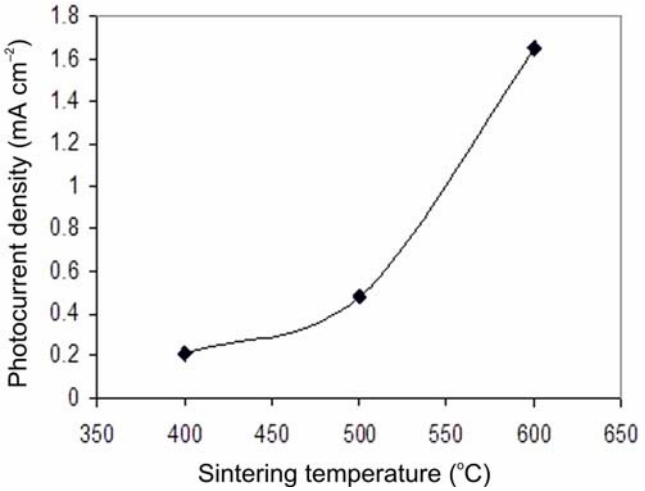

Figure 7. Photocurrent density recorded at 0·5 V bias with ZnO film sintered at different sintering temperatures.

Table 4. Open circuit potential (V_{oc}), short circuit current (J_{sc}) and fill factor (ff) recorded with illumination of zinc oxide film in PEC cell*.

Sintering temperature (°C)	V_{OC} (V)	J_{SC} (μA cm^{-2})	ff
	Mean ± SD	Mean ± SD	Mean ± SD
	Light		
400	0·40 ± 0·04	105 ± 18	0·20 ± 0·03
500	0·59 ± 0·06	361 ± 40	0·36 ± 0·04
600	0·71 ± 0·06	1321 ± 82	0·48 ± 0·03

* and S.D. : same as in table 1

Table 5. Flat band potential (V_{fb}) and charge carrier density (N_D) for zinc oxide films*.

Sintering temperature (°C)	V_{fb} (V)	$N_D \times 10^{-19}$ (cm^{-3})
	Mean ± SD	Mean ± SD
400	–0·38 ± 0·04	19 ± 6
500	–0·46 ± 0·05	15 ± 2
600	–0·51 ± 0·08	20 ± 5

* and SD: same as in table 1

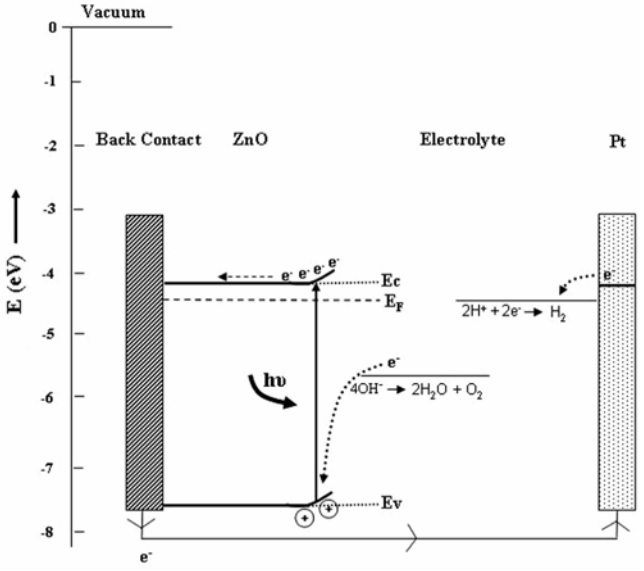

Figure 8. A tentative flow of electron in a PEC cell with ZnO working electrode.

pends upon the quantum selection rules for the particular material. A straight line (figure 5) is obtained, when $(\alpha h\nu)^2$ is plotted against photon energy ($h\nu$), which indicates that the absorption edge is due to a direct allowed transition ($n = 1$ for direct allowed transition). The intercept of the straight line on $h\nu$ axis corresponds to the optical bandgap (E_g) and its values determined for ZnO films are shown in table 3. The bandgap of films which were obtained after sintering at different sintering temperatures and, thus, had different microstructures, do not differ significantly. However, the bandgap values are in the expected range for ZnO thin films (Ashrafi and Jagdish 2007).

The current–voltage ($I - V$) characteristic curves of ZnO films in 0·1 M NaOH (pH 13) were recorded. The curves demonstrated a typical feature of n-type semiconductor electrodes. Table 4 depicts the open circuit voltage (V_{oc}), short circuit current (J_{sc}) and fill factor (ff), recorded under illumination with ZnO films. The variation of observed photocurrent density (i.e. $I_{illumination} - I_{darkness}$) with applied voltage is shown in figure 6, while figure 7 depicts the photocurrent density recorded at 500 mV bias voltage with ZnO films sintered at different temperatures. Since, there was no additional redox couple in the electrolyte, the significant value of photocurrent density can be attributed to electrochemical splitting of water, which was well indicated by evolution of gases in the form of bubbles on the electrode surface. The photocurrent density increased with increase in sintering temperature from 400–600°C.

ZnO, prepared in this study, with its bandgap in the range of 3·16–3·20 eV, seems to be an efficient material for the absorption of UV light, showing, at the same time, moderate to low absorption in the visible region, probably caused by defect states. It also appears that its band edges are seemingly well aligned to redox levels corresponding to hydrogen and oxygen evolution, which is indicated by significant short circuit current, especially with films sintered at 500 and 600°C. Although, in this study no efforts were made to determine the exact positions of conduction and valence band edges in ZnO, yet, utilizing the values reported in literature (Koffyberg and Benko 1982), a tentative flow of electrons in a PEC cell, comprising ZnO and Pt as working and counter electrodes, respectively, has been depicted in figure 8. It is clear from the figure that with ZnO as working electrode in PEC cell spontaneous electron flow is possible even without any external bias. However, it should be added here that with any change in bandgap or band edge positions, as a result of variations in electrolyte composition, the requirement of bias voltage may become necessary.

Generally, the flat band potential (V_{fb}) and carrier density (N_D) are determined by measuring the capacitance (C) of the electrode/electrolyte interface at different elec-

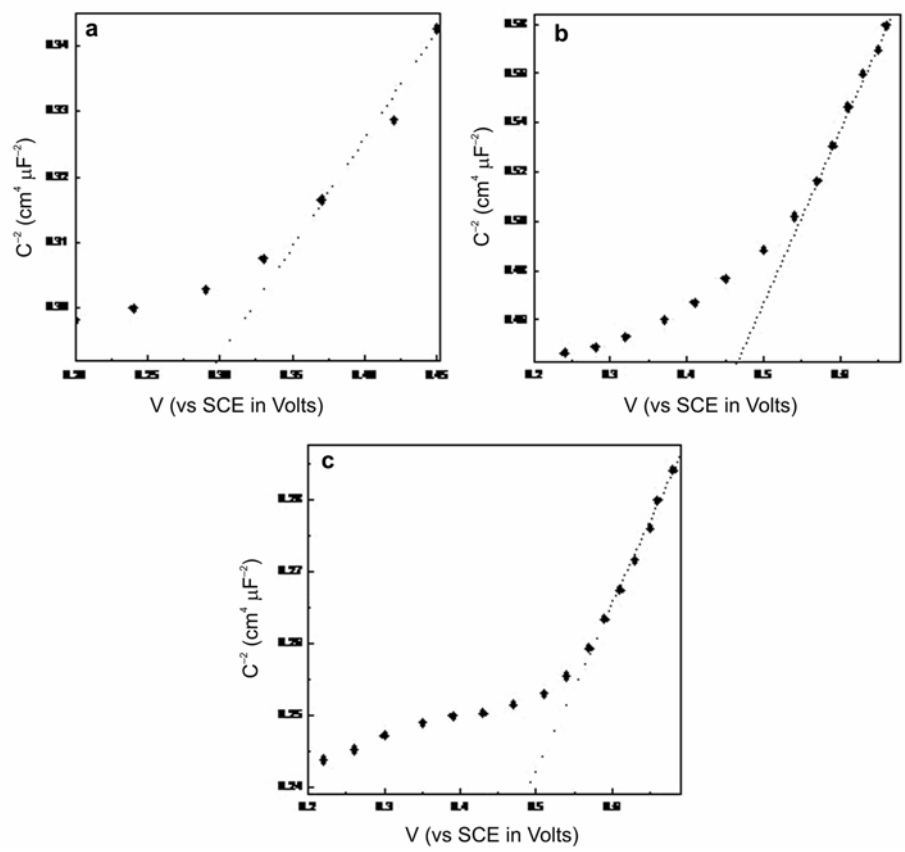

Figure 9. Mott–Schottky curves recorded with ZnO films sintered at **a**. 400, **b**. 500 and **c**. 600°C.

trode potentials (V) using (3) and (4) (Shinar and Kennedy 1982)

$$1/C^2 = [2/\varepsilon_0\,\varepsilon_s\,qN_D)][V - V_{fb} - (k_BT/q)], \quad (3)$$

$$S = 2/(\varepsilon_0\varepsilon_s qN_D), \quad (4)$$

where ε_0 and ε_s are permittivity of free space and semiconductor electrode, respectively, q the electronic charge, T the temperature in Kelvin, k_B the Boltzmann's constant, and S the slope of $1/C^2$ vs V i.e. Mott–Schottky (MS) curve. In this study, the capacitance at ZnO–NaOH junction was measured, with V varying from –1500 to 1500 mV, at 1 kHz signal frequency. The intercepts of the MS curves (figure 9, for films sintered at 400, 500 and 600°C) on the potential axis are considered as the values of V_{fb} and are depicted in table 5. The observed values of V_{fb}, which are negative, are comparable to the values reported earlier by some workers for ZnO (Ashrafi and Jagdish 2007). The measured potentials from the intercepts of MS curves, i.e. V_{fb}, are different from onset potentials, obtained from I^2 vs V relations. Such a deviation indicates the presence of surface states at the electrode–electrolyte interface, where carriers may recombine easily (Tafalla and Salvador 1989).

The typical maximum carrier concentration reported for the zincblende ZnO is ~10^{19} cm^{-3}, while for the wurtzite ZnO is ~ 10^{20} cm^{-3}, which means it is higher in the wurtzite ZnO (Ashrafi and Jagdish 2007). The measured carrier concentrations, in the samples prepared in this study, fall in the same range. Further, mixed evolution of both zincblende ZnO and wurtzite ZnO in the prepared samples is apparent from carrier concentration data also. For PEC application and current generation, apart from the concentration of carrier, their mobility is also important. Although, in this study no attempts were made to record carrier mobility in the samples, yet, it is a known fact that as the carriers travel through a semiconductor, they encounter various scattering mechanisms that govern the carrier mobility in the electronic system. Usually the carrier mobility is limited by the electron–electron as well as electron–phonon scattering. An order of magnitude fall in carrier concentration in zincblende ZnO, compared to wurtzite phase, is reportedly due to less contribution of impurities and/or higher structural symmetry (Ashrafi 2008). This implies that in the zincblende phase electron–impurity scattering and electron–phonon scattering are less than in wurtzite structure. Further, due to structural symmetry also electron mobility in zincblende ZnO is

relatively higher (Ashrafi and Jagdish 2007). Measured resistivity values of thin film samples, indicating lowest resistivity in samples sintered at 600°C, suggest higher carrier mobility. Observed higher photocurrent values with samples sintered at 600°C are, therefore, due to improved optical absorption coupled with decreased resistivity, and carrier mobility appears more critical than carrier concentration for use of ZnO in PEC splitting of water.

4. Conclusions

The present study, thus, leads to the following conclusions:
(I) Polytypic ZnO thin films, with mixed evolution of hexagonal wurtzite and cubic zincblende structures, have been obtained by using the preparatory method.
(II) Microstructure of the films changes on varying film preparation conditions, especially the sintering temperature.
(III) Observed absorption spectra and the optical band-gap of the films, measured by employing a UV-Vis scanning spectrophotometer suggest that the films are efficient UV absorber and moderate–weak absorber of visible light. Thus, their use for PEC splitting of water is possibile. However, use of appropriate dye-sensitizers would be helpful to expand absorption to higher wavelengths.
(IV) The films prepared at sintering temperature ≈ 600°C yield maximum photocurrent and are more efficient for photosplitting of water. This can be attributed to the better optical absorption and decreased electrical resistivity of the samples.

Acknowledgements

Research grant received from BRNS, Department of Atomic Energy, Govt. of India (No. 2007/37/44/BRNS) and UGC, Govt. of India (F. No. 30-36/2004(SR)) by one of the authors (RS), is gratefully acknowledged. We are also thankful to Dr Shyam Prasad, National Institute of Oceanography, Goa, for SEM analysis of samples.

References

Ahn B D, Oh S H, Lee C H, Kim G H, Kim H J and Lee S Y 2007 *J. Cryst. Growth* **309** 128
Agrawal A, Chaudhary Y S, Satsangi V R, Dass S and Shrivastav R 2003 *Curr. Sci.* **85** 371
Armelao L, Barreca D, Bertappelle M, Boltaro G, Sada C and Tondello E 2003 *Thin Solid Films* **442** 48
Ashrafi A and Jagdish C 2007 *J. Appl. Phys.* **102** 071101-1
Ashrafi A 2008 *J. Appl. Phys.* (in press) doi: 10.1016/j.apsusc.2008.070103
Chandra Babu K S, Srivastava O N and Subba Rao G V 1994 *Curr. Sci.* **66** 715
Chandra N, Wheeler B L and Bard A J 1985 *J. Phys. Chem.* **89** 5037
Chauhan D, Satsangi V R, Dass S and Shrivastav R 2006 *Bull. Mater. Sci.* **29** 709
Chaudhary Y S, Agrawal A, Shrivastav R, Satsangi V R and Dass S 2004 *Int. J. Hydrogen Energy* **29** 131
Djaoued Y, Phong V H, Badilescu S, Ashrit P V, Girouard F E and Truong V V 1997 *Thin Solid Films* **293** 108
Fu-Ren Fan F and Bard A J 1980 *J. Am. Chem. Soc.* **102** 3677
Kim S K, Jeong S Y and Cho C R 2003 *Appl. Phys. Lett.* **82** 562
Klug H P and Alexander L E 1974 *X-ray diffraction procedures for polycrystalline and amorphous materials* (New York: Wiley)
Koffyberg F P and Benko F A 1982 *J. Appl. Phys.* **53** 1173
Levy-Clement C, Lagoubi A, Neumann-Spullart M, Robot M and Tenne R 1991 *J. Electrochem. Soc.* **138** L69
Lu J G, Fujita S, Kawaharamura T and Nishinaka H 2007 *Chem. Phys. Lett.* **441** 68
Maruyama T 1998 *J. Electrochem. Soc.* **37** 4099
Morales J, Sanchez L, Martin F, Ramos-Barrado J R and Sanchez M 2005 *Thin Solid Films* **474** 133
Musat V, Rego A M, Monteiro R and Fortunato E 2008 *Thin Solid Films* **516** 1512
Oral A Y, Mensur E, Aslan M H and Basaran E 2004 *Mater. Chem. Phys.* **83** 140
Ray S C 2001 *Solar Energy Mater. Solar Cells* **68** 307
Salvador P, Guterrez C, Campet G and Hagenmuller P 1984 *J. Electrochem. Soc.* **131** 550
Sagar P, Kumar M and Mehra R M 2005 *Mater. Sci. – Poland* **23** 685
Shinar R and Kennedy J H 1982 *Solar Energy Mater.* **6** 323
Stilwell D E and Park S M 1982 *J. Electrochem. Soc.* **129** 1501
Tafalla D and Salvador D 1989 *J. Electroanal. Chem.* **270** 285
Wang J, Sallet V, Jomard F, Rego A M, Elamurugu E, Martins R and Fortunato E 2007 *Thin Solid Films* **515** 8785
Yoko T, Yuasa A, Kamiga K and Sakka S 1991 *J. Electrochem. Soc.* **138** 2279
Yoon K H and Chung K S 1992 *J. Appl. Phys.* **72** 5743